Chemistry–A European Journal
Research Article
doi.org/10.1002/chem.202200766
Chemistry Europe
European Chemical Societies Publishing
www.chemeurj.org

Pyrimidoquinazolinophenanthroline Opens Next Chapter in Design of Bridging Ligands for Artificial Photosynthesis**

Jannik Brückmann,[a] Carolin Müller,[b, c] Tamar Maisuradze,[b] Alexander K. Mengele,[a] Djawed Nauroozi,[a] Sven Fauth,[a] Andreas Gruber,[d] Stefanie Gräfe,[b] Kerstin Leopold,[d] Stephan Kupfer,[b] Benjamin Dietzek-Ivanšić,*[b, c] and Sven Rau*[a]

Abstract: The synthesis and detailed characterization of a new Ru polypyridine complex containing a heteroditopic bridging ligand with previously unexplored metal-metal distances is presented. Due to the twisted geometry of the novel ligand, the resultant division of the ligand in two distinct subunits leads to steady state as well as excited state properties of the corresponding mononuclear Ru(II) polypyridine complex resembling those of prototype $[Ru(bpy)_3]^{2+}$ (bpy = 2,2'-bipyridine). The localization of the initially optically excited and the nature of the long-lived excited states on the Ru-facing ligand spheres is evaluated by resonance Raman and fs-TA spectroscopy, respectively, and supported by DFT and TDDFT calculations. Coordination of a second metal (Zn or Rh) to the available bis-pyrimidyl-like coordination sphere strongly influences the frontier orbitals, apparent by, for example, luminescence quenching. Thus, the new bridging ligand motif offers electronic properties, which can be adjusted by the nature of the second metal center. Using the heterodinuclear Ru–Rh complex, visible light-driven reduction of NAD^+ to NADH was achieved, highlighting the potential of this system for photocatalytic applications.

Introduction

Light-induced electron transfer lies at the heart of photosynthesis, the most important chemical transformation process on earth.[1] Within artificial photosynthesis significant steps towards a deeper understanding of structural and electronic factors determining the efficiency of electron transfer rely on the interplay between advanced spectroscopic methods and the availability of suitable model systems.[2–5] Besides studying multi component systems for hydrogen evolution as for example shown in the seminal work by Lehn and Sauvage as early as 1977,[6] heterooligonuclear metal complexes containing specific bridging ligands (BLs), which determine the distance between the (photo)redox active metal centers, the degree of electronic coupling and the stability of the coordination centers have been pivotal for the development of supramolecular photocatalysts for water splitting.[7–10] Access to new BLs is therefore a key requirement to improve the understanding of fundamental aspects of light-induced electron transfer and at the same time enabling new applications in photocatalysis. Due to this, bridging systems of high rigidity with bipyridine- or phenanthroline-like coordination spheres providing sufficient stability were evaluated in numerous reports.[10–13] Representative examples (see Figure 1) of Ru complexes with increasing BL length would be the series of 2,2′-bipyrimidine (bpym),[14–16] 1,6,7,12-tetraazaperylene (tape, dipyrido[4,3,2-*de*:2′,3′,4′-*gh*][1,10]phenanthroline)[17–20] or eilatin (dibenzo[*b,j*]-dipyrido[4,3,2-*de*:2′,3′,4′-*gh*][1,10]phenanthroline)[17,21] -like structure and tetrapyrido[3,2-*a*:2′,3′-*c*:3′′,2′′-*h*:2′′′,3′′′-*j*]phenazine (tpphz)[9,22,23] which have been intensively studied. Several mono- and dinuclear complexes of those relays have been investigated.[9,15,19,20,23] For bpym- and tape-like dinuclear complexes relatively strong ground-state coupling between both metal centers has been observed whereas tpphz seems to largely decouple them.[19,24] Photocatalytic hydrogen formation with related Ru-BL-M catalysts (M = metal) is only observed with tpphz.[9] However, tpphz utilization is hampered by a low-lying phenazine-based orbital severely limiting the choice of reducible catalytic metal centers. Principal access to a BL with shorter

[a] J. Brückmann, Dr. A. K. Mengele, Dr. D. Nauroozi, S. Fauth, Prof. Dr. S. Rau
Institute of Inorganic Chemistry I
Ulm University
Albert-Einstein-Allee 11, 89081 Ulm (Germany)
E-mail: sven.rau@uni-ulm.de
[b] Dr. C. Müller, T. Maisuradze, Prof. Dr. S. Gräfe, Dr. S. Kupfer, Prof. Dr. B. Dietzek-Ivanšić
Institute of Physical Chemistry
Friedrich-Schiller University Jena
Helmholtzweg 4, 07743 Jena (Germany)
[c] Dr. C. Müller, Prof. Dr. B. Dietzek-Ivanšić
Leibniz Institute of Photonic Technology (IPHT) e.V.
Department Functional Interfaces
Albert-Einstein-Straße 9, 07745 Jena (Germany)
E-mail: benjamin.dietzek@leibniz-ipht.de
[d] A. Gruber, Prof. Dr. K. Leopold
Institute of Analytical and Bioanalytical Chemistry
Ulm University
Albert-Einstein-Allee 11, 89081 Ulm (Germany)

[**] A previous version of this manuscript has been deposited on a preprint server (https://doi.org/10.33774/chemrxiv-2021-bpd20).
Supporting information for this article is available on the WWW under https://doi.org/10.1002/chem.202200766

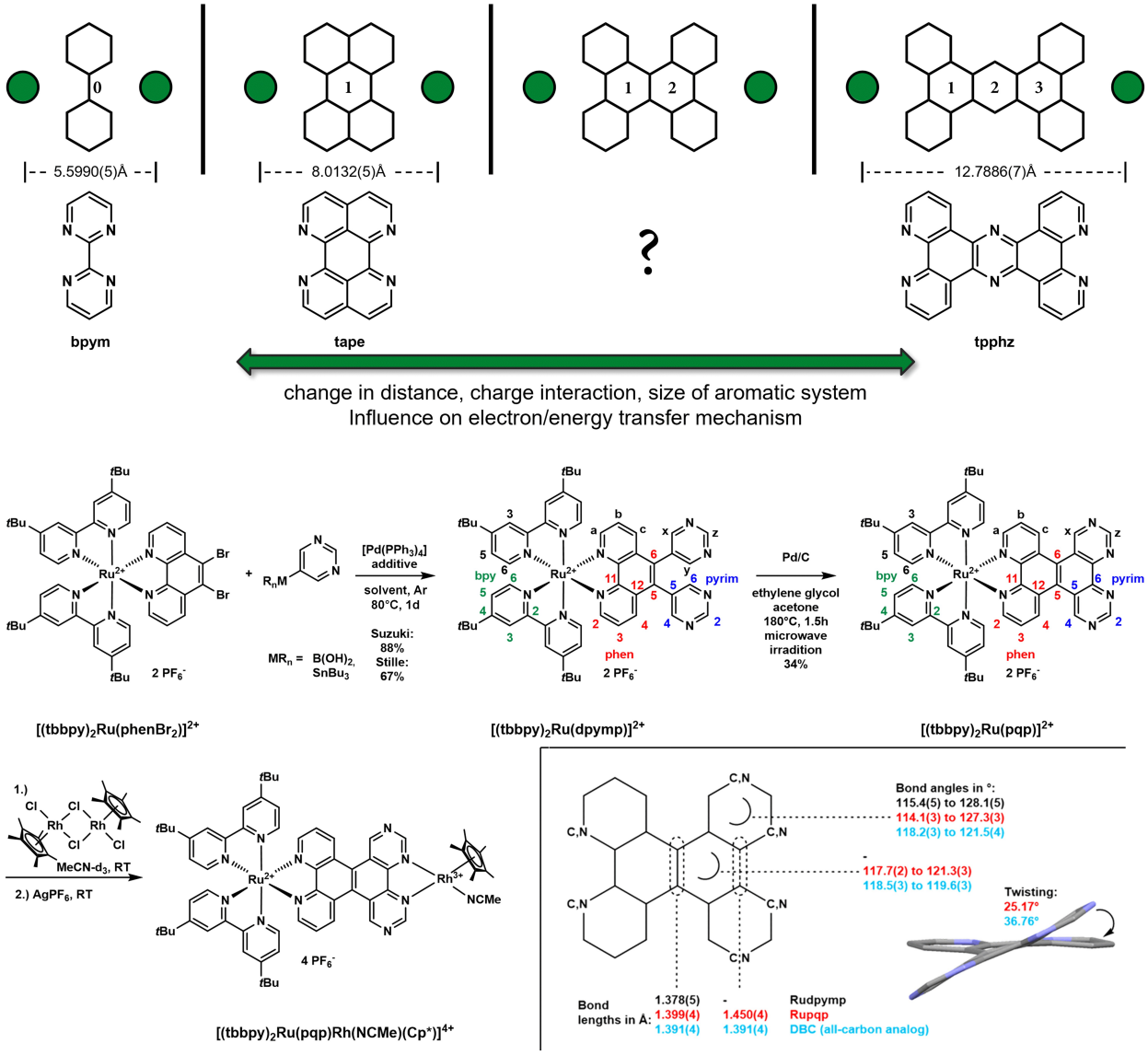

Figure 1. Top: Existent bridging ligand structures and selected metal-to-metal distances from solid state structures of $[(bpy)_2Ru(bpym)Ir(Cp^*)]^{2+}$,[16] $[(L)Ru(tape)Ru(L)]^{4+}$ (with L = N,N′-dimethyl-2,11-diaza-[3.3](2,6)-pyridinophane)[20] and $[(tbbpy)_2Rutpphz Ru(tbbpy)_2]^{4+}$ (tbbpy = 4,4′-di-*tert*-butyl-2,2′-bipyridine).[9] Bottom: Synthetic protocol and positions of the respective protons (in black) and carbon atoms (coloured; with ligand (sphere) abbreviations); inset shows a part of the all-carbon analog dibenzo[*g,p*]chrysene (DBC)[25] or pqp framework and the discussed bond angles/lengths and the twisting of Rupqp; color code: Rudpymp (black), Rupqp (red), DBC (light blue).

metal-to-metal distances and potentially sufficient degree of electronic decoupling can be derived starting from 5,6-disubstituted 1,10-phenanthrolines. Glazer and Tor presented synthetic concepts for dehydrogenative CC coupling chemistry in related systems,[17] which should enable a route towards the target unit. First, coupling of 5-substituted pyrimidine to a Ru(II) 1,10-phenanthroline (phen) system at its 5,6 positions via Pd-catalyzed cross-coupling reactions was performed (see Figure 1, center). This was followed by the construction of a conformationally rigid BL via Pd on charcoal-activated ring-closure procedure reported earlier.[17] Here we introduce this novel BL coordinated to a Ru(II) center to bridge the gap between existing systems. The synthesis is complemented by structural and electronic characterization via optical spectroscopy and quantum chemistry. Furthermore, its ability for coordination of a second metal center, *i.e.*, for future applications in the scope of photocatalysis, is explored.

Results and Discussion

The synthesis of Ru(II) polypyridine complexes bearing π-extended, N-heterocycle substituted phen type ligands was performed via two cross-coupling reactions at the dibrominated $RuphenBr_2$ (*i.e.* $[(tbbpy)_2Ru(phenBr_2)]^{2+}$; tbbpy = 4,4′-di-*tert*-butyl-2,2′-bipyridine; $phenBr_2$ = 5,6-dibromo-1,10-phenanthro-

line) precursor, followed by a thermal dehydrogenation reaction using palladium on charcoal (Pd/C). This chemistry-on-the-complex approach was selected, as different attempts to synthesise the free pqp ligand (pqp = pyrimido[5′,4′:7,8]quinazolino[5,6-*f*][1,10]phenanthroline) following previously published procedures failed,[26,27] possibly due to the electron deficient nature of the pyrimidyl groups.

Starting from the literature-known compound $RuphenBr_2$ either Suzuki or Stille reactions were used to form the 1,10-phenanthroline-5,6-bis-pyrimidine substituted complex Rudpymp ($[(tbbpy)_2Ru(dpymp)]^{2+}$; dpymp = 5,6-di(pyrimidin-5-yl)-1,10-phenanthroline). So far, literature examples on cross-coupling approaches with $phenBr_2$ only used electron-rich organometallic derivatives like donor-substituted phenyl or thiophene moieties.[28,29] Cross-coupling with acceptor-substituted, electron-deficient substrates or nitrogen heterocycles proved to be challenging for example due to mono-substitution.[26,30,31] Published reaction conditions for Stille cross-coupling ended up exclusively with mono-substitution and concomitant dehalogenation of the second halogen substituent.[29,32,33] The use of copper iodide as additive[34,35] led to di-substitution and Rudpymp in a yield of up to 67%. Suzuki cross-coupling with standard reaction conditions[28] gave excellent yields up to 88%.

To achieve a fully ring-closed system of the bis-pyrimidyl substituted phen moiety, dehydrogenation reactions were conducted. Literature-known cyclization with Pd/C in ethylene glycol and acetone under elevated temperatures gave an NMR-detectable amount of Rupqp ($[(tbbpy)_2Ru(pqp)]^{2+}$).

Improving the reaction conditions (additive(s), temperature, time; see chapter 3.4 in the Supporting Information) and running the reaction in a microwave setup significantly increased yields (from NMR-detectable to 34% yield). Strikingly, the reaction was not possible using Rudpymp obtained under Stille conditions. In total reflection X-ray fluorescence spectroscopy (TXRF) significant residues of copper and iodide could be detected (see Figure S66). The inhibiting effect of CuI on the cyclization reaction was verified by adding CuI to the Suzuki product (see Figures S37 and S38).

Upon ring closure, Rupqp offers a second coordination sphere, which emerges as an electron deficient 4,4′-bipyrimidyl-like environment. To evaluate the ability to attach a second metal center to Rupqp, we decided to use the [Rh(Cp*)(X)] (Cp* = pentamethylcyclopentadienyl, X = Cl, solvent) fragment. Earlier reports accomplished the coordination by simply stirring both the BL containing Ru-complex and the Rh(III) dimer $[Rh(Cp^*)Cl_2]_2$ in solution of for example methanol or methylene chloride (see Figure 1), the latter was applied for example for $[(tbbpy)_2Ru(tpphz)]^{2+}$ (*i.e.* Rutpphz).[36–38] Within this work, this attempt yielded only partial conversion. Follow-up purification steps with solvents with donor capability, ended in partial chlorido ligand substitution by the solvent. Due to this ligand lability, earlier described methods were used to cleave the chlorido ligand quantitatively by addition of silver hexafluorophosphate.[39] To exclude insoluble silver chloride, several centrifugations and re-crystallizations were done. Possibly due to soluble silver clusters,[40] atomic absorption spectrometry (AAS) still reveals silver contaminations for $[(tbbpy)_2Ru(pqp)Rh(NCMe)(Cp^*)]^{4+}$ (RupqpRh) (see Figure S67).

For the ^1H NMR spectra of Rudpymp and Rupqp, the signal pattern is simplified upon ring closure (see Figure 2). This is due to the long-range coupling of protons x and y, which causes – in addition to proton z – a second singlet to appear (see Figures 1 and 2 for the assignment). All pyrimidine protons and the c protons of the phen sphere are considerably shifting downfield due to ring-closing (maximal 1.5 ppm for H_x) and further upon Rh(III) coordination. This trend diminishes progressively when moving from the inner ligand sphere to the adjacent phen/pyrimidyl positions and the peripheral tbbpy.

Compared to complexes bearing shorter (e.g. $[(bpy)_2Ru(tape)]^{2+}$[19]) and longer (e.g. Rutpphz[41]) BLs, Rudpymp and Rupqp show no concentration dependence in acetonitrile within a concentration range of 1.3 mM to 30.3 or 18.5 mM, respectively (see Figures S23 and S24).

Single crystal analysis

The solid-state structures of Rudpymp and Rupqp shown in Figure 3 reveal typical bite angles of 78.19(9)° to 79.6(1)° for the tbbpy ligands and 78.5(1)° (Rudpymp, for more details see the Supporting Information) or 78.33(9)° (Rupqp) for the novel ligand moiety.

Rupqp exhibits shortening of the bonds between the phen (C5 and C6, see Figure 1) and pyrimidyl units (C5). Bond lengths decrease from *min.* 1.490(5) Å to *max.* 1.459(4) Å. Similar to the all-carbon analog DBC (1.391 Å[25]), the C5–C6 bond of the phen moiety (1.399(4) Å) is in the range of typical benzene-like sp^2-sp^2 hybridized, aromatic C–C bonds of about 1.40 Å.[42] In addition, both pqp and DBC reveal a slightly longer bond length (1.450(4) Å) between the aromatic rings in the backbone (each C6 atom of the pyrimidyl units, see Table S3). Possibly due to steric pressure between the hydrogens at the x position of the pyrimidine and c of the phen, a tilted geometry of the pqp can be found in the solid-state structure. In agreement with the DFT results (29.5°, Tables S3 and S6), a torsion angle of 25.17° is observed. DBC-like derivatives resembling pqp reveal even higher twisting of 29.95–44.95°.[43,44] Noteworthy, the pqp

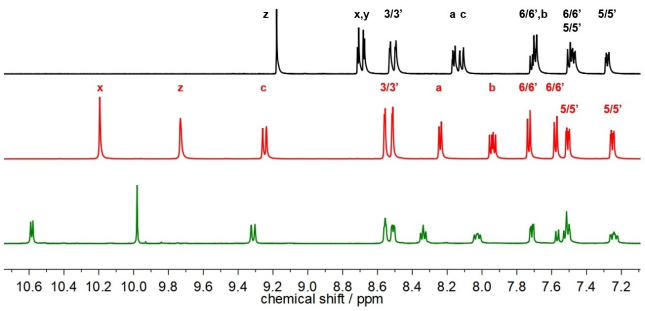

Figure 2. ^1H NMR spectra of Rudpymp (top), Rupqp (middle) and RupqpRh (bottom) in acetonitrile-d_3 (due to absence of concentration dependence as shown in Figures S23 and S24 no specific concentrations were used).

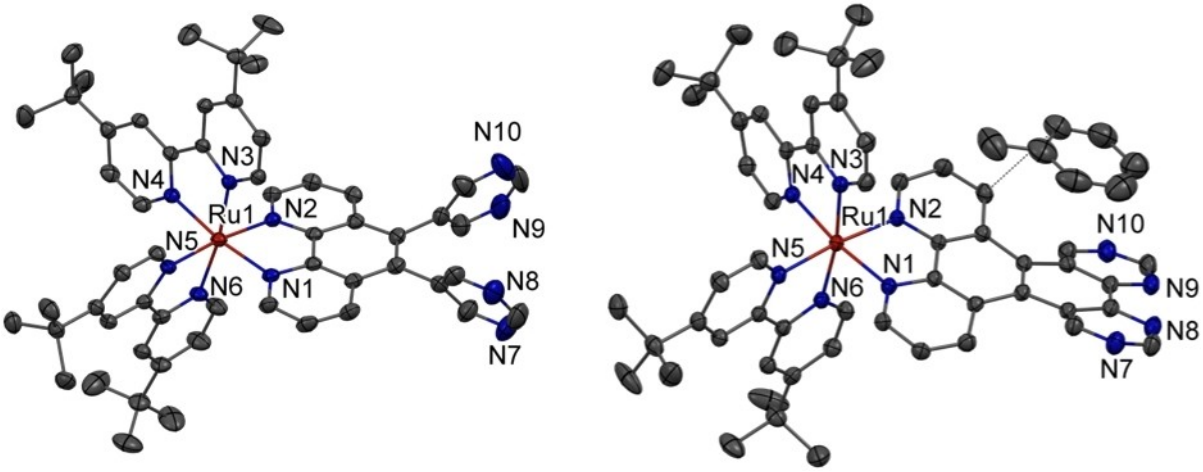

Figure 3. Solid-state structure of Rudpymp (left) and Rupqp (right) (thermal ellipsoids are drawn at a probability level of 50%). Hydrogen atoms, PF_6^- counter anions and solvent molecules are omitted for clarity; additionally, intermolecular Rupqp-toluene interactions are depicted.

ligand reveals stacking with co-crystallized toluene solvent molecule with a distance of 3.267(6) Å (see Figure 3).

Electrochemistry

Consistent with literature, the reversible Ru(II)/(III) oxidation of Rudpymp and Rupqp appears being insensitive to the substitution of phen and ring closure at around 0.8 V (Figure 4).[28] RupqpRh exhibits a reversible Ru(II)-based oxidation at anodically shifted potentials of 0.91 V. The four cathodic events of Rudpymp are reversible or quasi-reversible. Assuming no effect of the new dpymp ligand on the tbbpy ligands, the redox events at potentials of −1.95 V and −2.37 V are assigned to the latter according to literature.[28] The one-electron reduction of bare pyrimidine takes place at rather negative potentials.[45] Hence, the first reductive event of Rudpymp at −1.67 V is based on the phen moiety. This reduction is shifted anodically by ca. 100 to 120 mV compared to similar complexes (see Table 1).[28,46]

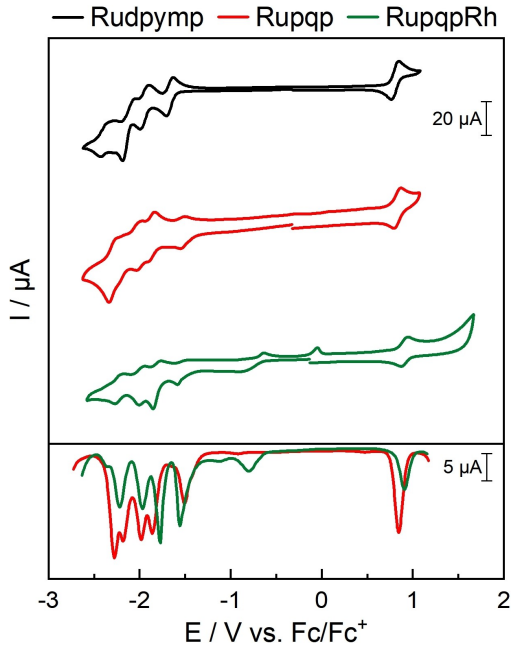

Figure 4. Cyclic voltammograms (top) and differential pulse voltammograms (bottom) of Rudpymp (black), Rupqp (red) and RupqpRh (green) in acetonitrile (1 mM) referenced against the Fc/Fc^+ couple. Conditions: scan rate 100 mVs^{-1} (black, green), 200 mVs^{-1} (red), $[Bu_4N][PF_6]$ at 0.1 M as supporting electrolyte.

For Rupqp, five reduction events emerge (see also DPV in Figure 4). Thus, the fifth reduction is likely localized on the new BL architecture and can be either ascribed to the novel central sphere within the pqp ligand or an accessible, second reduction of the pyrimidine units. The coordination of the second metal sphere, *i.e.* Rh(Cp*), induces additional changes. First, due to the Rh(III) metal center, two reduction events at −0.80 and −1.12 V appear. They emerge at similar potentials as for $[Rh(bpm)(Cp^*)Cl]^+$ (bpm = 4,4′-bipyrimidine, see Table 1), where a two-fold reduction takes place. In accordance with literature, the Rh center displays two consecutive reduction steps in case of an acetonitrile coordinated species.[47] In addition, the $[Rh(bpm)(Cp^*)Cl]^+$ motive of RupqpRh is notably easier to reduce than a N-poorer $[Rh(phen)(Cp^*)Cl]^+$ motive.[37] Such a system would have been obtained if pyridyl groups instead of pyrimidyl groups would have been reacted with $RuphenBr_2$.

Second, all subsequent ligand-based reductions emerge at similar potentials as for Rupqp. Only the fifth reduction of Rupqp is shifted considerably in RupqpRh and lies outside of the accessible potential window or it just appears as the small shoulder visible at high cathodic potentials in the CV and DPV (see Figure 4). Interestingly, the Ru(II)/(III) oxidation shifts anodically by 80 mV, hinting to a more electron deficient Ru(II) center comparable to $[(bpy)_2Ru(bpm)]^{2+}$ ($E^{1/2}_{ox} = 1.05$ V),[48] suggesting an increased influence of the Rh(III) metal center due to the shorter BL. For Rutpphz and RutpphzRh ($[(tbbpy)_2Ru(tpphz)Rh(Cp^*)Cl]^{3+}$) only a 30 mV anodic shift of

Table 1. Electrochemical and spectroscopic properties of Rudpymp, Rupqp and RupqpRh together with suitable substances for comparison. * shoulder.

Compound	$E^{1/2}_{ox}$/V	$E^{1/2}_{red}$/V	λ(abs,max)/nm (ε [10^3 $M^{-1}cm^{-1}$]	λ(em,max)/ nm	Φ(em, Ar)/ Φ(em, air)
$[(tbbpy)_3Ru]^{2+}$ [28,54]	0.73	−1.82, −2.02, −2.28	451 (13)	607	9.5% / 1.8%
$[(tbbpy)_2Ru(phen)]^{2+}$ [46]	0.74	−1.77, −1.98, −2.25	454 (16.0)	610	–
$[(tbbpy)_2Ru(phenBr_2)]^{2+}$ [28]	0.85	−1.79, −2.00, −2.32	449 (14.3)	631	–
Rudpymp	0.81	−1.67, −1.95, −2.18, −2.37	451 (19.1), 336 (8.16), 285 (78.2)	631	16% / 1%
Rupqp	0.83	−1.53, −1.86, −2.01, −2.19, −2.29	452 (18.8), 336 (17.4), 282 (117)	637	12% / 1%
RupqpRh	0.91	−0.80, −1.12,* −1.56, −1.77, −1.97, −2.22, −2.36*	542, 451, 336, 285	637	2% / 0%
$[Rh(bpm)(Cp^*)(Cl)]^+$ [37]		−0.92	375, 364	–	–

the the Ru(II)/(III) couple was observed due to coordination of Rh(III).[38]

Characterization of the Franck-Condon region

To study the Franck-Condon region, we employ steady state absorption and resonance Raman (rR) spectroscopy supported by TDDFT.

UV/vis absorption

The absorption spectrum of Rudpymp (Figure 5) shows a narrow absorption band at 286 nm (78.2×10^3 $M^{-1}cm^{-1}$), a weaker shoulder between 300 and 380 nm and a broad, featureless metal-to-ligand charge-transfer (MLCT) absorption band peaking at 451 nm (19.1×10^3 $M^{-1}cm^{-1}$). Such spectra are typical for $[(tbbpy)_2Ru(phen)]^{2+}$ (Ruphen)-type complexes, *i.e.*, where the phen-moiety is substituted in the 5- and 6-position.[28,29] The underlying transitions are summarized in Table S7 and Figure S72.

While the difference between oxidation and reduction potentials in Rudpymp and Rupqp (2.48 eV or 2.36 eV, see Table 1) is smaller than in the parent complex Ruphen (2.58 eV), the MLCT absorption maxima of both complexes are at around 450 nm. This mismatch between electrochemical and spectroscopic findings indicates the presence of low-energy acceptor states on the dpymp and pqp ligand,[49] namely in the proximal ($MLCT_{pqp}$: S_7, and S_8; $MLCT_{bpy}$: S_{10} and S_{12}) and distal ligand sphere ($MLCT_{dpymp}$: S_1) as outlined in Tables S7 and S9.

The corresponding acceptor orbitals participate in the electrochemical process but the associated transitions have vanishing oscillator strengths, for example, S_1 of $MLCT_{dpymp}$ character at 2.38 eV (520 nm, f = 0.001). Hence, the $MLCT_{bpy}$ and $MLCT_{phen}$ transitions dominate the absorption spectrum of Rudpymp and Rupqp, explaining the similarity to the absorption data of Ruphen. Thus, also other Ru complexes bearing variably 5,6-substituted phen ligands show ^{1}MLCT maxima at very similar wavelengths as Rudpymp.[28,46,50]

Upon ring closure, the molar absorptivity of the MLCT absorption band remains essentially unchanged, while the band at 280 nm (increase by a factor of 1.5) and the shoulders between 300 and 380 nm (increase by a factor of 2.1) become more prominent. TDDFT associates the enhanced absorption at 280 nm with the increased oscillator strength of the ππ* excitation of the pqp ligand upon ring C–C bond formation (Rupqp: S_{58}, $f = 0.514$ *versus* Rudpymp: S_{66}, $f = 0.371$).

The MLCT band maximum of Rupqp is not shifted with respect to Rudpymp, which is counterintuitive in view of the ring-annulated π-extension of the phen-ligand, *i.e.*, in comparison to $[(bpy)_2Ru(L)]^{2+}$-type complexes of Rudape (dape = diazaperylene),[17] Rutape[17,19,20] or Rueilatin[21] where significant bathochromic shifts of the MLCT absorption bands have been observed. In contrast to these shorter π-extended ligands, Rupqp reveals a non-planar pqp ligand potentially decreasing π-conjugation.

Resonance Raman

To further explore the multiple MLCT transitions, rR spectra were collected upon excitation in the red and blue flank of the MLCT absorption band, *i.e.*, at 405 and 473 nm (see Figure 5).[51] The rR spectra of Rudpymp are composed of modes associated to the tbbpy ligands as well as the phen and pyrimidyl units of the dpymp ligand, respectively. By direct comparison to the homoleptic reference compound $[Ru(tbbpy)_3]^{2+}$ and the parental complex Ruphen, we assign the modes at 1036, 1319, 1483, 1540 and 1609 cm^{-1} to the tbbpy ligand sphere. The vibrations centered at 1515 and 1585 cm^{-1} are assigned to phen-associated modes.[52,53] The rR modes at 1200, 1262 and 1465 cm^{-1} are assigned to the pyrimidyl sphere (py), indicating the population of $MLCT_{py}$ states. Thus, the rR data supports the initial excitation – as provided by TDDFT – of $MLCT_{bpy}$ as well as two low-lying MLCT states ($MLCT_{phen}$ and $MLCT_{py}$) on the dpymp ligand, respectively. The $MLCT_{phen}$ gain in relative weight compared to $MLCT_{tbbpy}$ states upon shifting the excitation wavelength from 405 to 473 nm, in agreement with TDDFT (see Figure 5).

The rR spectra of Rupqp exhibit similar vibrational modes associated with the tbbpy (1036, 1212, 1319, 1483, 1540, 1615 cm^{-1}) and pqp ligand (1262, 1543, 1576 and 1600 cm^{-1}). In direct comparison to Rudpymp, the phen-type modes at 1515 and 1585 cm^{-1} vanish (473 nm excitation).

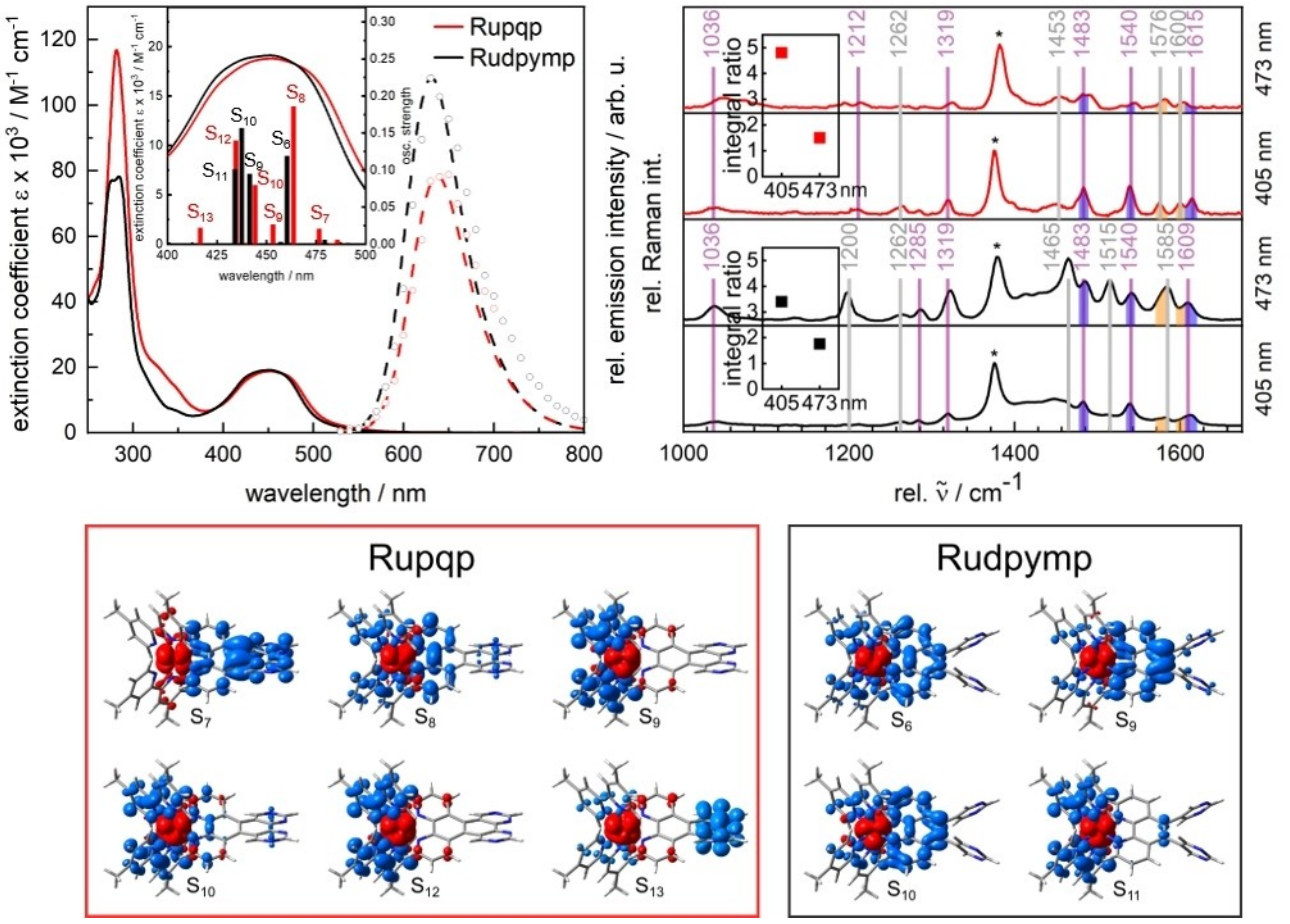

Figure 5. Top left: Extinction coefficients of Rudpymp (black) and Rupqp (red) with relative emissions (dashed) intensities (λ(ex) = 451 nm), simulated transitions underlying the absorption bands are indicated in the inlet; top right: rR spectra of Rudpymp (black) and Rupqp (red) upon 405 nm (bottom) and 473 nm (top) excitation in acetonitrile. The tbbpy-, and dpymp- or pqp-type modes are indicated by violet and grey bars, respectively. The integral ratios of selected modes (tbbpy in blue relative to dpymp/pqp in orange) for the respective excitation wavelength are included as insets for Rupqp and Rudpymp; integral values are normalized to the integral of the modes of Rudpymp upon 405 nm excitation, respectively; bottom: transitions of Rudpymp and Rupqp visualized by charge density differences; charge transfer occurs from red to blue.

However, the integral ratio of the tbbpy-to-dpymp/pqp-type modes (between 1470 and 1620 cm^{-1}) is approximately 1.5 for both, Rudpymp and Rupqp at 473 nm excitation. This indicates similar contributions of the phen acceptor orbital to the Franck-Condon region. Consistent with Rudpymp, the contribution of the pqp ligand to the formation of the initially excited states increases upon shifting the excitation wavelength from 405 to 473 nm. This is reflected in the decrease of the ratio taken between the integral of the tbbpy (1483, 1540, 1615 cm^{-1}) and pqp-type (1576 and 1600 cm^{-1}) modes by a factor of *circa* 2 (see Figure 5). TDDFT supports this trend, revealing low-lying MLCT states with pyrimidyl acceptor orbitals (e.g., S_7, see Figure 5).

Characterization of the long-lived excited states

The long-lived excited states are explored by emission spectroscopy. The emission band maximum of Rudpymp (λ(ex) = 420 nm) is located at 631 nm, which is red-shifted with respect to Ruphen (610 nm) but agrees with $RuphenBr_2$ (631 nm). This indicates that the pyrimidyl substituents influence the π-system of the phen system.[29]

Upon ring-closure (forming Rupqp), the emission maximum is shifted bathochromically by 18 meV to 637 nm. The comparably high emission quantum yield of 16% for Rudpymp decreases to 12% (Rupqp) (see Figure 5). DFT assigns the emissive state in Rudpymp and Rupqp to a $^3MLCT_{phen}$ state (dpymp: 647 nm, 1.92 eV, pqp: 657 nm, 1.89 eV), while the slight bathochromic shift (DFT: 30 meV) is associated with the increased π-system upon C–C bond formation (Figure S89).

The emission lifetimes of the complexes are 140 ns (Rudpymp) and 170 ns (Rupqp, 420 nm excitation in aerated acetonitrile). Overall, the findings indicate that both, Rudpymp and Rupqp, show emission from a long-lived ^3MLCT state, with excess electron density in the proximal ligand sphere, *i.e.*, on the tbbpy ligands and the phen moiety of dpymp and pqp, respectively. The triplet nature of the lowest-lying excited state is corroborated by its sensitivity to oxygen (see Figures S52 and

S53). Emission intensities of both complexes decrease significantly upon aeration (Φ(em) = 1 % for Rudpymp and Rupqp).

Photoinduced dynamics

Ultrafast transient absorption (fs-TA) spectra were collected upon 400 nm excitation of Rudpymp and Rupqp in acetonitrile. The data reveal a strong ground-state bleach (GSB) between 400 and 500 nm (Figure 6). The GSB accompanies strong excited-state absorption (ESA) centered at 350 nm (Rudpymp) or 340 nm (Rupqp) and a broad, spectrally flat ESA at wavelengths longer than 510 nm. The latter features are associated with $\pi\pi^*$ transitions on the reduced tbbpy and phen moieties and ligand-to-metal charge-transfer (LMCT) transitions (> 500 nm).

In Rudpymp, the ESA between 510 and 560 nm is more pronounced than in Rupqp. The assignment of ESA features is supported by TDDFT calculated dipole and spin-allowed transitions of the relaxed triplet states (^{3}MLCT): The predictions reveal that the ESA of the long-lived ^{3}MLCT states of Rudpymp and Rupqp, mainly stems from $\pi\pi^*$ and LMCT transitions. Moreover, TDDFT supports the absence of bridge-centered $\pi\pi^*$ states which are typically found for structurally related complexes like Rutpphz.[55–57] This hints towards a higher contribution of the phen moiety on the formation of the excited states in Rudpymp compared to Rupqp and agrees with the rR spectroscopic findings, revealing strong phen-type vibrational modes for Rudpymp, which are absent in the rR spectra of Rupqp.

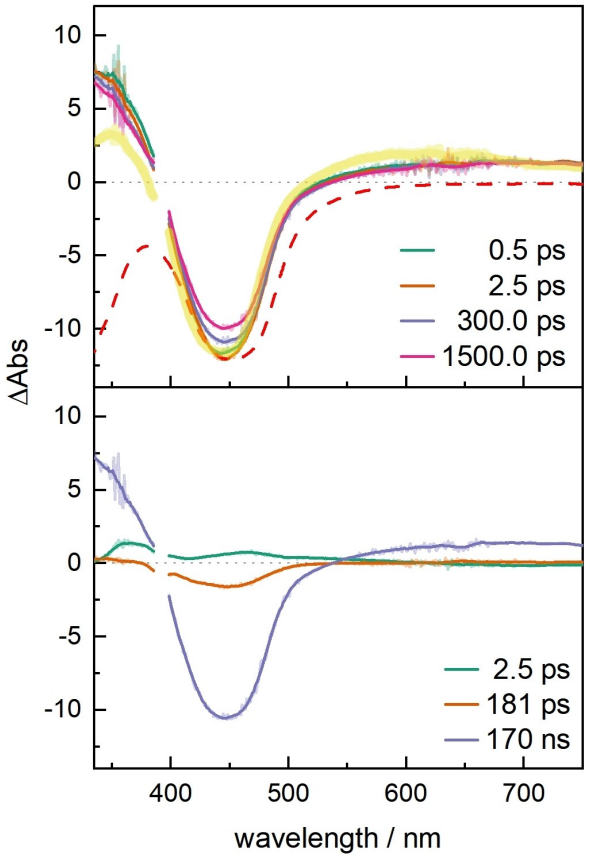

Figure 6. Ultrafast transient absorption (top) and decay-associated spectra (bottom) of Rupqp. The red, dashed line in the upper panel shows the scaled and inverted ground state absorption spectrum. For comparison the transient absorption spectrum of Rudpymp collected at a delay time of 1.5 ns is shown in yellow. The spectra are collected upon 400 nm excitation (excitation densities of *circa* 5 %) in a delay time range between 0.3 and 2 ns in acetonitrile. The lifetime of the long-lived state is obtained from nanosecond time-resolved emission spectroscopy (see Figures S70 and S71).

For both complexes the decay of the sub-ns signals is described by two time constants, namely τ_1 = 2.2 ps and τ_2 = 134 ps (Rudpymp) or τ_1 = 2.5 ps and τ_2 = 181 ps (Rupqp), respectively. The corresponding decay associated spectra (DAS, Figure 6 bottom) are qualitatively identical for Rudpymp and Rupqp. Hence, we will discuss the excited-state relaxation of both complexes in the framework of the same model.

The spectral changes associated with τ_1 (see DAS(τ_1)) are associated with intersystem crossing and vibrational cooling of the initially populated MLCT states[58–61] as manifested in the decay of ESA at around 380 nm due to $\pi\pi^*$ transitions on the reduced tbbpy. This causes the blue-shift of the ESA below 400 nm. Consequently, a thermalized ^{3}MLCT$_{phen}$ is formed. τ_2 describes the subsequent formation of the long-lived ^{3}MLCT state. This is associated with minor spectral changes in the ESA, however with a partial recovery of GSB features between 400 and 500 nm. We associate these findings with a non-radiative decay of a subset of both, ^{3}MC (metal-centered) and ^{3}MLCT$_{py}$ states.[62] Ultimately, a long-lived excited ^{3}MLCT state, with excess electron density on the tbbpy ligands (Rupqp) or both, the phen and tbbpy moieties (Rudpymp) is populated. The increased contributions of the phen moiety on the long-lived excited state agrees with the blue-shift of the emission maximum of Rudpymp compared to Rupqp.

pqp as bridging ligand - formation of dinuclear complexes and explorative light-driven redox catalysis

Upon coordination of [Rh(III)(Cp*)(X)] to the BL-containing complex Rupqp a shoulder at 520 nm emerges in the absorption spectrum - in line with quantum chemical calculations (Figure S85). Molecular orbitals available for MLCT$_{pqp}$ transitions at long wavelengths (S_6 in Table S12) from Ru(II) to the pq-sphere of the pqp ligand are energetically stabilized (2.26 eV) compared to Rupqp (2.55 eV). Possibly due to high contributions of the bis-pyrimidyl moiety, the excited state subsequently deactivates radiationless by electron transfer to the appended Rh(III) center.

Compared to Rupqp coordination of Rh leads to further attenuation of the emission quantum yield from 12 % (Rupqp) to 2 % (RupqpRh) (see Figure 7, red to green).

Similarly, addition of redox-inactive Zn(BF_4)$_2$ to Rupqp quenches the emission (Figure 7) as has been observed for Rutpphz complexes.[63,64] Opposite to Rh(III), Zn(II) induces inverse changes in the frontier orbitals of ground and excited states associated with the pqp ligand (see Figures 7 and S83 and S88; MO in Figure 7 is located at slightly higher energies

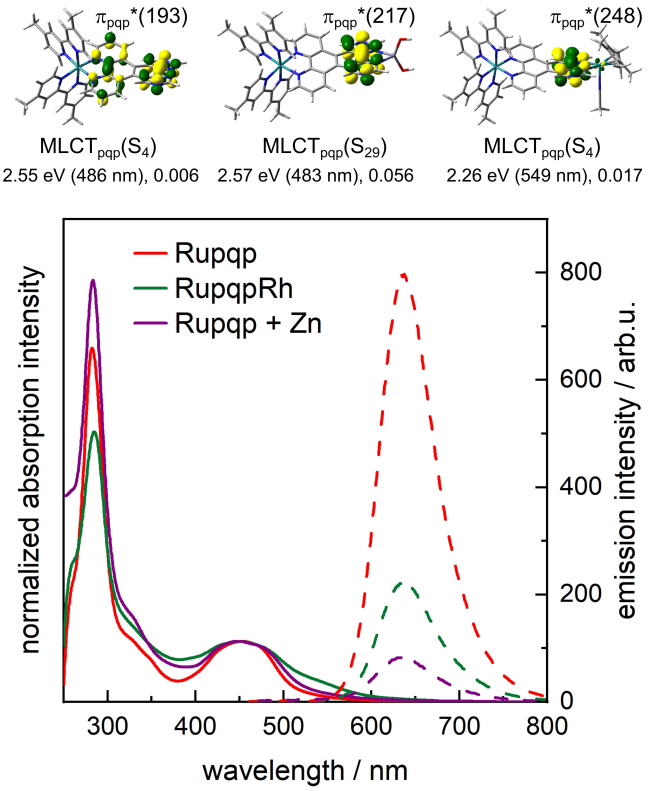

Figure 7. Top: excitation energies, wavelengths and oscillator strengths of low-lying MLCT$_{pqp}$ excitations and involved π_{pqp}* for Rupqp (S$_4$), RupqpZn (S$_{29}$) and RupqpRh (S$_4$); bottom: absorption and emission spectra of Rupqp, RupqpRh and Rupqp + [Zn(BF$_4$)$_2$]; absorption spectra were normalized at 451 nm; emission spectra were recorded upon excitation at 451 nm (OD 0.1).

than for Rupqp), *i.e.* with the spin density of the lowest triplet state centered on the Ru(III) and the adjacent phen-sphere. Possibly, the predominant excited state localization on the phen part of the pqp ligand enhances charge recombination and thus effective quenching of the ^{3}MLCT emission occurs.

From both Rh(III) and Zn(II) coordination it becomes clear that the order of the frontier orbitals of Rupqp can be altered depending on the respective second metal center. Thus, the pqp appears to be split into two halves with either phen and/or pyrimidyl contributions. Compared to the situation with Rupqp, addition of Zn(II) to Rudpymp does not alter absorption or emission behaviour (see Figures S55 and S56). Therefore, the ring closure is required for the interaction with a second metal center.

Finally, we investigated RupqpRh for its use in redox catalysis. Due to the silver contamination found by AAS, all catalytic experiments were accompanied by control experiments with addition of $AgPF_6$.

First, the principal ability of the RhCp* fragment to run formate-driven, chemical catalysis for reduction of nicotinamide co-factor NAD$^+$ was investigated (see mechanism reported in literature[65–67] and the Supporting Information for detailed experimental conditions). To further exclude an effect of the mononuclear complex on the reduction to NADH, Rupqp was investigated as well (see Figures S96 and S97). In presence of formate (room temperature, 40 °C, 50 °C), only RupqpRh shows conversion of NAD$^+$ to NADH (visible by the increasing absorbance at 340 nm and emission at 460 nm in Figure S94). As depicted in Figure S92, with increasing temperature, the catalysis is significantly faster and reaches a plateau already at slightly less than 50% conversion.

As the Rh center offers the possibility to run redox catalysis, the dinuclear complex was subjected to conditions where the catalytically competent Rh(I) intermediate can be formed photochemically (λ(ex) = 470 nm). As it can be seen in Figure S93, the two-fold reduced Ru(II)pqpRh(I) dyad can be built up upon illumination in presence of triethylamine as indicated by the appearance of a characteristic absorption band centered at around 760 nm.[37,56] The band which is ascribed to a Rh(I)→pqp MLCT transition is bathochromically shifted by about 100 nm compared to RutpphzRh due to the more electron withdrawing nature of the pqp ligand.[38] As light-induced reduction was successful with RupqpRh, electron transfer from Ru towards Rh can be expected.

Lastly, we examined if the light-driven Rh(III)/(I) conversion can be accompanied with the reduction of nicotinamide co-factor NAD$^+$ (Figure 8). In phosphate-buffered solution containing triethylamine as electron donor, the dyad RupqpRh was irradiated with blue light. RupqpRh again was the only catalytically active compound tested in this series of experiments. All other control experiments revealed either radical-mediated product formation of NAD$_2$[68] by Rupqp or Rupqp with addition of silver hexafluorophosphate (Figures S96–S97, TON(NADH) < 1) or no conversion for [Ru(tbbpy)$_3$]$^{2+}$ (Figure S98, TON(NADH) < 1). With elevated temperatures, the conversion with RupqpRh is progressively enhanced (Figure 8). An increase

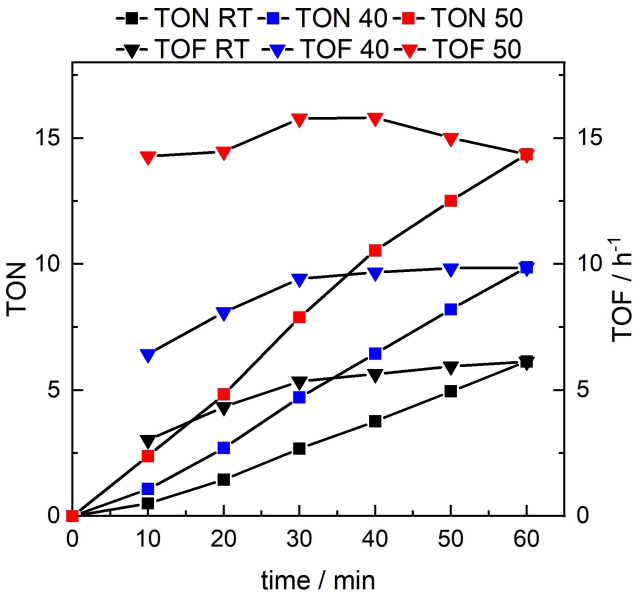

Figure 8. Light-induced redox catalysis of RupqpRh at room temperature (black), 40 °C (blue) and 50 °C (red) in water/acetonitrile mixtures (4:1, *v:v*); concentrations used RupqpRh (5 μM), NAD$^+$ (200 μM), TEA (0.12 M) and NaH_2PO_4 (0.1 M), excitation with 470 nm (50 mWcm^{-2}).

in turnover number for NADH from 5 (RT) to 10 (40 °C) and 15 (50 °C) can be observed.

Lastly, by comparing the performance of RupqpRh for formate-driven thermal (Figure S92) and light-driven (Figure 8) NADH-formation, it is clear that the thermal process results in higher TONs within 60 min and at all temperatures investigated. However, compared to structurally similar RuRh complexes, RupqpRh is capable to outperform for example those during light-driven NADH formation that contain a triazole group within the bridging ligand.[69] This is remarkable as the principal catalytic activity for NAD^+-reduction of RupqpRh is only ca. 50 % of these reference complexes as evaluated by the formate-driven process. It thus highlights the beneficial impact of the new pqp ligand on dinuclear systems for photocatalytic applications.

Moreover, also the most similar intermolecular system consisting of $[(tbbpy)_2Ru(phen)](PF_6)_2$ and [(bpm)Rh(Cp*)Cl]Cl[37] was tested for its light-driven catalytic activity. When using both complexes at 5 μM concentrations as in the experiments with RupqpRh, only TONs below 2 were obtained for the intermolecular system, irrespective whether the catalytic process was performed at room temperature or at 40 °C (Figure S100). The notably lower photostability of $[(tbbpy)_2Ru(phen)](PF_6)_2$ compared to RupqpRh during photocatalysis (Figures S95 and S100) is a clear disadvantage of the intermolecular approach. Additionally, no evidence of luminescence quenching between excited $[(tbbpy)_2Ru(phen)](PF_6)_2$ and [(bpm)Rh(Cp*)Cl]Cl was found. Both independent factors are capable to explain the insufficient performance of the intermolecular system (Figure S101). Thus, bridging the Ru- and the Rh-center by the new pqp-ligand has a beneficial impact on the photocatalytic activity of the individual moieties.

Experimental Section

Deposition Number(s) 2111036 (for Rudpymp) and 2111037 (for Rupqp) contain the supplementary crystallographic data for this paper. These data are provided free of charge by the joint Cambridge Crystallographic Data Centre and Fachinformationszentrum Karlsruhe Access Structures service.

Conclusion

Pyrimidoquinazolinophenanthroline, pqp, has been synthesized and proven to function as a new bridging ligand fostering light-driven catalysis. This novel bridging ligand was accessed via a dehydrogenative chemistry on the Ru-complex approach fusing two pyrimidine spheres via a geminate C–C-bond. The respective pyrimidine units were introduced to a Ru(II)phenBr_2 moiety using Suzuki or Stille cross coupling beforehand. From a structural point of view, the resultant Ru polypyridine complex Rupqp fills the gap of previously reported tape- and tpphz-based systems as it exhibits two central aromatic rings rather than one or three, respectively. In view of the broad range of possible heterocycles that can be introduced by the cross-coupling reactions utilized in the present study, a targeted design of photocatalysts featuring pqp-like ligands seems possible. Due to the twisted nature of the novel bridging ligand that has been revealed by scXRD as well as DFT methods, the steady-state as well as the excited-state properties resemble those of prototype $[Ru(bpy)_3]^{2+}$. This is explained by theoretical investigations and detailed, time-resolved photophysical studies, suggesting a subdivision of the pqp bridging ligand into two weakly coupled subunits. However, the energetics of the orbitals on the pqp ligand can be significantly influenced by coordination of a second metal center. The coordination of both, Zn(II) and Rh(III), lead to a quenching of the luminescence due to a redistribution of the frontier orbitals. These promising results point towards a coordination-induced switching of excited-state localization of Rupqp. Furthermore, the introduction of Rh(III)(Cp*) - yielding RupqpRh - renders access to visible light-driven photocatalytic reduction of naturally occurring nicotinamide NAD^+ to NADH. As the nature of the coordinated metal determines the location of excited states to a large degree, further exploitation towards tuneable photocatalysis will be possible.

Acknowledgements

We acknowledge funding by the DFG (German Research Foundation) - Projektnummer 364549901 - TRR 234 [A1 and C5]. J.B. was supported by the *Fonds der Chemischen Industrie* (*FCI*) and T.M. thanks the DAAD (German Academic Exchange Service) for a study scholarship for graduates (91733810). The authors gratefully acknowledge Andrea Hainthaler for the time-resolved emission measurements, Ilse Friedländer for rR measurements and Dominik Blaimer for GFAAS measurements. Open Access funding enabled and organized by Projekt DEAL.

Conflict of Interest

The authors declare no conflict of interest.

Data Availability Statement

The data that support the findings of this study are available in the supplementary material of this article.

Keywords: artificial photosynthesis · bridging ligand · light-induced redox catalysis · quantum chemistry · ruthenium photosensitizer

[1] W. W. Fischer, J. Hemp, J. E. Johnson, *Annu. Rev. Earth Planet. Sci.* **2016**, *44*, 647–683.
[2] D. F. Harrison, E. Weissberger, H. Taube, *Science* **1968**, *159*, 320–322.
[3] C. Creutz, H. Taube, *J. Am. Chem. Soc.* **1969**, *91*, 3988–3989.
[4] C. Creutz, H. Taube, *J. Am. Chem. Soc.* **1973**, *95*, 1086–1094.
[5] V. Balzani, G. Bergamini, F. Marchioni, P. Ceroni, *Coord. Chem. Rev.* **2006**, *250*, 1254–1266.
[6] J. M. Lehn, J. P. Sauvage, *Nouv. J. Chim.* **1979**, *1*, 449–451.

[7] L. De Cola, F. Barigelletti, V. Balzani, P. Belser, A. von Zelewsky, C. Seel, M. Frank, F. Vögtle, *Coord. Chem. Rev.* **1991**, *111*, 255–260.
[8] H. Ozawa, M. A. Haga, K. Sakai, *J. Am. Chem. Soc.* **2006**, *128*, 4926–4927.
[9] S. Rau, B. Schäfer, D. Gleich, E. Anders, M. Rudolph, M. Friedrich, H. Görls, W. Henry, J. G. Vos, *Angew. Chem. Int. Ed.* **2006**, *45*, 6215–6218; *Angew. Chem.* **2006**, *118*, 6361–6364.
[10] G. F. Manbeck, K. J. Brewer, *Coord. Chem. Rev.* **2013**, *257*, 1660–1675.
[11] S. Serroni, S. Campagna, F. Puntoriero, C. Di Pietro, N. D. Mc Clenaghan, F. Loiseau, *Chem. Soc. Rev.* **2001**, *30*, 367–375.
[12] M. Schulz, M. Karnahl, M. Schwalbe, J. G. Vos, *Coord. Chem. Rev.* **2012**, *256*, 1682–1705.
[13] G. Li, D. Zhu, X. Wang, Z. Su, M. R. Bryce, *Chem. Soc. Rev.* **2020**, *49*, 765–838.
[14] M. Hunziker, A. Ludi, *J. Am. Chem. Soc.* **1977**, *99*, 7370–7371.
[15] S. Ernst, V. Kasack, W. Kaim, *Inorg. Chem.* **1988**, *27*, 1146–1148.
[16] K. R. Brereton, C. L. Pitman, T. R. Cundari, A. J. M. Miller, *Inorg. Chem.* **2016**, *55*, 12042–12051.
[17] E. C. Glazer, Y. Tor, *Angew. Chem. Int. Ed.* **2002**, *41*, 4022–4026; *Angew. Chem.* **2002**, *114*, 4194–4198.
[18] A. Chouai, S. E. Wicke, C. Turro, J. Bacsa, K. R. Dunbar, D. Wang, R. P. Thummel, *Inorg. Chem.* **2005**, *44*, 5996–6003.
[19] T. Brietzke, W. Mickler, A. Kelling, H. J. Holdt, *Dalton Trans.* **2012**, *41*, 2788–2797.
[20] T. Brietzke, W. Mickler, A. Kelling, U. Schilde, H. J. Krüger, H. J. Holdt, *Eur. J. Inorg. Chem.* **2012**, 4632–4643.
[21] D. Gut, A. Rudi, J. Kopilov, I. Goldberg, M. Kol, *J. Am. Chem. Soc.* **2002**, *124*, 5449–5456.
[22] J. Bolger, A. Gourdon, E. Ishow, J.-P. Launay, *Inorg. Chem.* **1996**, *1669*, 2937–2944.
[23] M. G. Pfeffer, B. Schäfer, G. Smolentsev, J. Uhlig, E. Nazarenko, J. Guthmuller, C. Kuhnt, M. Wächtler, B. Dietzek, V. Sundström, et al., *Angew. Chem. Int. Ed.* **2015**, *54*, 5044–5048; *Angew. Chem.* **2015**, *127*, 5132–5136.
[24] D. P. Rillema, K. B. Mack, *Inorg. Chem.* **1982**, *21*, 3849–3854.
[25] F. H. Herbstein, *Acta Crystallogr. Sect. B* **1979**, *35*, 1661–1670.
[26] F. Doettinger, Y. Yang, M. A. Schmid, W. Frey, M. Karnahl, S. Tschierlei, *Inorg. Chem.* **2021**, *60*, 5391–5401.
[27] G. E. Shillito, S. E. Bodman, J. I. Mapley, C. M. Fitchett, K. C. Gordon, *Inorg. Chem.* **2020**, *59*, 16967–16975.
[28] A. Stumper, T. D. Pilz, M. Schaub, H. Görls, D. Sorsche, K. Peuntinger, D. Guldi, S. Rau, *Eur. J. Inorg. Chem.* **2017**, *2017*, 3799–3810.
[29] J. Brückmann, A. A. Heidecker, D. Popovic, A. K. Mengele, D. Nauroozi, P. Bäuerle, S. Rau, *Eur. J. Inorg. Chem.* **2019**, *2019*, 1832–1838.
[30] N. Kudo, M. Perseghini, G. C. Fu, *Angew. Chem. Int. Ed.* **2006**, *45*, 1282–1284; *Angew. Chem.* **2006**, *118*, 1304–1306.
[31] L. C. Campeau, K. Fagnou, *Chem. Soc. Rev.* **2007**, *36*, 1058–1068.
[32] L. Jedinák, R. Zátopková, H. Zemánková, A. Šustková, P. Cankař, *J. Org. Chem.* **2017**, *82*, 157–169.
[33] J. Sherwood, J. H. Clark, I. J. S. Fairlamb, J. M. Slattery, *Green Chem.* **2019**, *21*, 2164–2213.
[34] L. S. Liebeskind, R. W. Fengl, *J. Org. Chem.* **1990**, *55*, 5359–5364.
[35] V. Farina, S. Kapadia, B. Krishnan, C. Wang, L. S. Liebeskind, *J. Org. Chem.* **1994**, *59*, 5905–5911.
[36] U. Kölle, M. Grätzel, *Angew. Chem. Int. Ed. Engl.* **1987**, *26*, 567–570, *Angew. Chem.* **1987**, *99*, 572–574.
[37] M. Ladwig, W. Kaim, *J. Organomet. Chem.* **1991**, *419*, 233–243.
[38] A. K. Mengele, S. Kaufhold, C. Streb, S. Rau, *Dalton Trans.* **2016**, *45*, 6612–6618.
[39] C. White, A. Yates, P. M. Maitlis, *Inorg. Synth.* **1992**, *29*, 228–234.
[40] S. Kaufhold, L. Petermann, D. Sorsche, S. Rau, *Chem. Eur. J.* **2017**, *23*, 2271–2274.
[41] M. G. Pfeffer, C. Pehlken, R. Staehle, D. Sorsche, C. Streb, S. Rau, *Dalton Trans.* **2014**, *43*, 13307–13315.
[42] R. C. Fortenberry, C. M. Novak, T. J. Lee, P. P. Bera, J. E. Rice, *ACS Omega* **2018**, *3*, 16035–16039.
[43] X. S. Ke, Y. Hong, V. M. Lynch, D. Kim, J. L. Sessler, *J. Am. Chem. Soc.* **2018**, *140*, 7579–7586.
[44] N. Yoshida, S. Kamiguchi, K. Sakao, R. Akasaka, Y. Fujii, T. Maruyama, T. Iwasawa, *Tetrahedron Lett.* **2020**, *61*, 152033.
[45] J. E. O'Reilly, P. J. Elving, *J. Am. Chem. Soc.* **1971**, *93*, 1871–1879.
[46] B. Schäfer, H. Görls, S. Meyer, W. Henry, J. G. Vos, S. Rau, *Eur. J. Inorg. Chem.* **2007**, 4056–4063.
[47] J. A. Hopkins, D. Lionetti, V. W. Day, J. D. Blakemore, *Organometallics* **2019**, *38*, 1300–1310.
[48] S. D. Ernst, W. Kaim, *Inorg. Chem.* **1989**, *28*, 1520–1528.
[49] S. Campagna, F. Puntoriero, F. Nastasi, G. Bergamini, V. Balzani, *Top. Curr. Chem.* **2007**, *280*, 117-214.
[50] P. Wintergerst, A. K. Mengele, D. Nauroozi, S. Tschierlei, S. Rau, *Eur. J. Inorg. Chem.* **2019**, *2019*, 1988–1992.
[51] M. Wächtler, J. Guthmuller, L. González, B. Dietzek, *Coord. Chem. Rev.* **2012**, *256*, 1479–1508.
[52] C. V. Kumar, J. K. Barton, I. R. Gould, N. J. Turro, J. Van Houten, *Inorg. Chem.* **1988**, *27*, 648–651.
[53] M. Karnahl, S. Krieck, H. Görls, S. Tschierlei, M. Schmitt, J. Popp, D. Chartrand, G. S. Hanan, R. Groarke, J. G. Vos, et al., *Eur. J. Inorg. Chem.* **2009**, 4962–4971..
[54] K. Suzuki, A. Kobayashi, S. Kaneko, K. Takehira, T. Yoshihara, H. Ishida, Y. Shiina, S. Oishi, S. Tobita, *Phys. Chem. Chem. Phys.* **2009**, *11*, 9850–9860.
[55] L. Zedler, J. Guthmuller, I. Rabelo de Moraes, S. Kupfer, S. Krieck, M. Schmitt, J. Popp, S. Rau, B. Dietzek, *Chem. Commun.* **2014**, *50*, 5227–5229.
[56] L. Zedler, A. K. Mengele, K. M. Ziems, Y. Zhang, M. Wächtler, S. Gräfe, T. Pascher, S. Rau, S. Kupfer, B. Dietzek, *Angew. Chem. Int. Ed.* **2019**, *58*, 13140–13148; *Angew. Chem.* **2019**, *131*, 13274–13282.
[57] M. Martynow, S. Kupfer, S. Rau, J. Guthmuller, *Phys. Chem. Chem. Phys.* **2019**, *21*, 9052–9060.
[58] R. A. Malone, D. F. Kelley, *J. Chem. Phys.* **1991**, *95*, 8970–8976.
[59] N. H. Damrauer, G. Cerulla, A. Yeh, T. R. Boussie, C. V. Shank, J. K. McCusker, *Science* **1997**, *275*, 54–57.
[60] S. Wallin, J. Davidsson, J. Modin, L. Hammarström, *J. Phys. Chem. A* **2005**, *109*, 4697–4704.
[61] C. W. Stark, W. J. Schreier, J. Lucon, E. Edwards, T. Douglas, B. Kohler, *J. Phys. Chem. A* **2015**, *119*, 4813–4824.
[62] J. Olofsson, B. Önfelt, P. Lincoln, *J. Phys. Chem. A* **2004**, *108*, 4391–4398.
[63] S. A. Tysoe, R. Kopelman, D. Schelzig, *Inorg. Chem.* **1999**, *38*, 5196–5197.
[64] Y. Liu, A. Chouai, N. N. Degtyareva, D. A. Lutterman, K. R. Dunbar, *J. Am. Chem. Soc.* **2005**, *127*, 10796–10797.
[65] H. C. Lo, C. Leiva, O. Buriez, J. B. Kerr, M. M. Olmstead, R. H. Fish, *Inorg. Chem.* **2001**, *40*, 6705–6716.
[66] C. L. Pitman, O. N. L. Finster, A. J. M. Miller, *Chem. Commun.* **2016**, *52*, 9105–9108.
[67] A. Marrone, R. H. Fish, *J. Organomet. Chem.* **2021**, *943*, 121810.
[68] T. Golaś, E. Bojarska, B. Czochralska, *J. Photochem. Photobiol. A* **1990**, *54*, 333–347.
[69] L. Zedler, P. Wintergerst, A. K. Mengele, C. Müller, C. Li, B. Dietzek-Ivanšić, S. Rau, *Nat. Commun.* **2022**, *13*, 2538.

Manuscript received: May 13, 2022
Accepted manuscript online: June 20, 2022
Version of record online: July 26, 2022